AIAA-86-1084
Transonic Potential Flow Calculations
by Two Artificial Density Methods

G. Volpe, Grumman Corp.,
Bethpage, NY, and A. Jameson,
Princeton Univ., Princeton, NJ

AIAA/ASME 4th Fluid Mechanics, Plasma Dynamics and Lasers Conference
May 12-14, 1986/Atlanta, GA

TRANSONIC POTENTIAL FLOW CALCULATIONS
BY TWO ARTIFICIAL DENSITY METHODS

G. Volpe*
Grumman Corporate Research Center
Bethpage, NY 11714

and

A. Jameson**
Department of Mechanical and Aerospace Engineering
Princeton University
Princeton, NJ 08544

Abstract

A steady transonic flow over an airfoil is computed by solving the full potential equation discretized over a contour-fitting grid in full conservation form. Near shock waves, the density is corrected to account for the rise in entropy in the region. A multigrid alternating direction method is used to drive the iteration. In supersonic flow regions, artificial dissipation is introduced either by a flux biasing scheme or by a density biasing scheme. The two schemes are second order accurate, while the density biasing scheme is second order accurate throughout the flow field except for a small region near shock waves. Results of calculations with the two schemes show that the flux biasing scheme gives a sharper resolution of the shock than the density biasing scheme when the shock itself is weak. As shock strength increases, the shock-capturing abilities of the two schemes become equal. Throughout the range of cases tested, the two schemes exhibited comparable speed and robustness.

I. Introduction

The transonic full potential equation is still a very useful and very competitive model for describing the flow over an airfoil at transonic speeds.   Very efficient algorithms have been developed for its solution, in particular by Jameson[1] and Holst.[2]   The algorithm devised by Jameson, known as FLO36, has also been coupled with a viscous interaction method by Melnik et al,[3] thus resulting in a widely used tool for computing the viscous transonic flow over airfoils.   In all shock-capturing methods, artificial dissipation has to be introduced in regions of supersonic flow to account for the hyperbolicity of the equation there.   Dissipation can be added either by the addition of an artificial viscosity term as shown in Ref. 1 or by retarding the density as demonstrated in Ref. 4.   To enhance the stability of numerical schemes employing one of these forms of artificial dissipation, the second author found that the dissipation had to be activated at a Mach number slightly below one.   In addition, second order accurate spatial differencing could not be maintained near shock waves.   The accuracy of the schemes had to be reduced to first order there. These two factors contributed to smear the shock over some mesh intervals, the number of which depended on the shock strength.

More recently Boerstoel[5] and Hafez et al[6] have introduced algorithms which use an artificial dissipation based on flux biasing. These methods follow from a flux splitting scheme described by Engquist and Osher[7] which specifically rules out expansion shocks. Osher et al[8] proved this rigorously for two-dimensional flow and also showed that, at least for one-dimensional flow, a compression shock could be captured within one mesh interval.   In principle, then, it should be possible to get a sharper shock definition with flux biasing since there is no need to switch on the artificial dissipation below the sonic Mach number and no need to reduce spatial accuracy near a shock. The other advantage is that there is no need to define parameters to control when the dissipation is to be activated.

In this paper, second order spatially accurate artificial dissipation forms based on both flux biasing and density biasing are presented. Except for the dissipation terms, the discretization of the full potential equation is otherwise identical in the two methods. The discretized equations are solved via a multigrid alternating direction (MAD) algorithm first described by Jameson in Ref. 1.

II. Numerical Method

The equation we seek to solve is the continuity equation

$$\frac{\partial}{\partial x}(\rho u) + \frac{\partial}{\partial y}(\rho v) = 0 \qquad (1)$$

where x and y are Cartesian coordinates, ρ is the density, and u and v are the two velocity components. Assuming irrotationality, these can be expressed as components of the potential function ϕ

$$u = \phi_x \quad , \quad v = \phi_y \qquad (2)$$

The actual computations are carried out in a region obtained by conformally mapping the exterior of the airfoil in question onto the interior of a circle. A uniform polar coordinate mesh, described by r and θ, then gives an excellent discretization of the flow field. In the mapped plane, the flow equation becomes

$$\frac{\partial}{\partial \theta}(\rho U) + r \frac{\partial}{\partial r}(\rho V) = 0 \qquad (3)$$

---

* Staff Scientist, Member AIAA
** Professor

where

$$U = \phi_\theta \quad , \quad V = r\,\phi_r \qquad (4)$$

and the physical velocity components in the two coordinate directions are

$$u = \frac{rU}{H} \quad , \quad v = \frac{rV}{H} \qquad (5)$$

where H is the modulus of the transformation to the exterior of the circle.

As described in Ref. 1, at a mesh point i,j in *the flow field, Eq (3) is discretized as*

$$\frac{1}{\Delta\theta^2}\left[\rho_{i+1/2,j}U_{i+1/2,j} - \rho_{i-1/2,j}U_{i-1/2,j}\right]$$

$$+ \frac{r_j}{\Delta r^2}\left[\rho_{i,j+1/2}V_{i,j+1/2} - \rho_{i,j-1/2}V_{i,j-1/2}\right] = 0$$

$$(6)$$

where

$$U_{i+1/2,j} = \phi_{i+1,j} - \phi_{i,j} \qquad (7a)$$

$$V_{i,j+1/2} = r_{j+1/2}(\phi_{i,j+1} - \phi_{i,j}) \qquad (7b)$$

with similar expressions for $U_{i-1/2,j}$ and $V_{i,j-1/2}$. Here i+1/2 and j+1/2 denote values at midpoints of a mesh interval. The density ρ is computed at cell centers. Hence,

$$\rho_{i+1/2,j} = \frac{1}{2}\left(\rho_{i+1/2,j+1/2} + \rho_{i+1/2,j-1/2}\right)$$

$$(8)$$

At supersonic points, artificial dissipation is introduced by modifying the density in Eq (6).

Density Biasing

At supersonic points, the density term, ρ, in the first bracket in Eq (6) is replaced by a density which is biased in the upstream direction according to the density gradient; call this $\hat{\rho}$. Thus assuming the flow to be in the direction of increasing i, we take

$$\hat{\rho}_{i+1/2,j} = \rho_{i+1/2,j} - \mu_{ij}\,\Delta\theta\,\left(\frac{\partial\rho}{\partial\theta}\right)_{i,j} \qquad (9)$$

A similar expression holds for $\rho_{i-1/2,j}$. Similarly the density terms in the second bracket of Eq (6) are replaced by a biased density, $\tilde{\rho}$, which is taken to be

$$\tilde{\rho}_{i,j+1/2} = \rho_{i,j+1/2} - \mu_{ij}\,\Delta r\,\left(\frac{\partial\rho}{\partial r}\right)_{i,j} \qquad (10)$$

In Eq (9) and (10), we define

$$\mu_{ij} = \text{Max}\left[0,\ \nu_1\left(1 - \frac{M_c^2}{M^2}\right)\right] \qquad (11)$$

where M is the local Mach number and M_c^2 is a user-defined parameter slightly less than one, typically 0.9. ν_1 is another user-defined parameter usually set at one. In our scheme, the density is evaluated at each of the cell centers. Thus $\left(\frac{\partial\rho}{\partial\theta}\right)_{i,j}$ and $\left(\frac{\partial\rho}{\partial r}\right)_{i,j}$ at the mesh point i,j can be evaluated from averaged differences of the densities at the encircling cell centers. Thus, for example

$$\left(\frac{\partial\rho}{\partial\theta}\right)_{ij} = \frac{1}{2}\left(\rho_{i+1/2,j+1/2} + \rho_{i+1/2,j-1/2}\right.$$

$$\left. - \rho_{i-1/2,j+1/2} - \rho_{i-1/2,j-1/2}\right) \qquad (12)$$

Application of Eq (9) and (10) results in a spatially first order accurate scheme in supersonic regions. Second order accuracy can be recovered by defining

$$\hat{\rho}_{i+1/2,j} = \rho_{i+1/2,j} - \mu_{ij}\,\Delta\theta\left[\left(\frac{\partial\rho}{\partial\theta}\right)_{i,j} - \varepsilon_{ij}\left(\frac{\partial\rho}{\partial\theta}\right)_{i-1,j}\right]$$

$$(13)$$

and taking $\varepsilon_{ij} = 1$. *The numerical scheme, however, proved unstable unless* ε_{ij} *is made zero near shock waves. A straightforward way of implementing this is to define*

$$\varepsilon_{ij} = \text{Max}\left(0,\ \nu_2 - \nu_3\left|\Delta\theta\left(\frac{\partial\rho}{\partial\theta}\right)_{ij} + \Delta r\left(\frac{\partial\rho}{\partial r}\right)_{ij}\right|\right) \quad (14)$$

When ν_2 is zero, the scheme is first order accurate in supersonic regions. For $\nu_2 = 1$ partial second accuracy is introduced. ν_3 is a parameter of order one defined by the user. An expression similar to Eq (13) defines $\tilde{\rho}_{i,j+1/2}$.

Flux Biasing

An alternate method of introducing artificial dissipation in the numerical scheme is by retarding the density based on the flux. Thus, in both brackets of Eq (6) we substitute the density ρ with a retarded density $\hat{\rho}$ defined as

$$\hat{\rho} = \rho - \frac{\Delta s}{q}\frac{\partial F}{\partial s} \qquad (15)$$

2

with

$$F = \rho q \qquad \text{for} \qquad M > 1$$

$$= \rho^* q^* \qquad \text{for} \qquad M < 1 \qquad (16)$$

where q represents the total velocity, s represents the streamwise direction, and the asterisk denotes sonic conditions. The quantity F, as ρ and q, is evaluated at each cell center. The streamwise gradient is broken up into components in the coordinate directions by

$$\Delta s \frac{\partial F}{\partial s} = \frac{u}{q} \Delta\theta \frac{\partial F}{\partial \theta} + \frac{v}{q} \Delta r \frac{\partial F}{\partial r} \qquad (17)$$

In our numerical scheme, this leads to the following representation for the retarded density terms we define at cell centers

$$\hat{\rho}_{i+1/2,j+1/2} = \rho_{i+1/2,j+1/2}$$

$$- [(\frac{u}{q^2}) \Delta\theta (\frac{\partial F}{\partial\theta}) + (\frac{v}{q^2}) \Delta r (\frac{\partial F}{\partial r})]_{i+1/2, j+1/2} \qquad (18)$$

Second order accurate approximations for the gradients in Eq (18) are given by

$$\Delta\theta(\frac{\partial F}{\partial\theta})_{i+1/2,j+1/2} = F_{i+1/2,j+1/2} - F_{i-1/2,j+1/2}$$

$$- \varepsilon_{i,j}(F_{i-1/2,j+1/2} - F_{i-3/2,j+1/2}) \qquad (19)$$

where ε_{ij} is given by Eq (14). A similar expression holds for $(\frac{\partial F}{\partial r})_{i+1/2,j+1/2}$.

The obvious advantage of this scheme is that the dissipation is switched on when the local Mach number is unity rather than a smaller subsonic value. The density biasing scheme is not stable with $M_c^2 = 1$.

Entropy Correction

Shocks computed by a potential flow scheme such as the present one tend to be stronger and, for airfoil flows, are usually located downstream of the location computed by a solution to the Euler equations. Hafez and Lovell[9] devised a method to account for the entropy rise through a shock within the context of a potential formulation. Thus, following Hafez and Lovell, at a mesh point just downstream of a shock, the density is multiplied by a factor proportional to the entropy rise through the shock, $\Delta S/R$. For a normal shock and with flow in the direction of increasing i,

$$\rho_{i+1/2,j+1/2} \rightarrow \rho_{i+1/2,j+1/2} e^{-\Delta S/R}$$

where

$$\frac{\Delta S}{R} = 2.5 [\log (\frac{7M_1^2-1}{6}) - \frac{7}{5} (\frac{6M_1^2}{M_1^2+5})] \qquad (20)$$

M_1 is the Mach number computed two points upstream of the shock.

This results in a correction to the residual to the potential equation, as represented by Eq (6), equal to

$$\Delta Res = \frac{1}{\Delta\theta} (e^{\Delta S/R}-1) \rho_{i+1/2,j} U_{i+1/2,j}$$

$$(21)$$

Iteration Scheme

The difference equations obtained with either scheme are solved by the MAD algorithm described in Ref. 1. This method employs a multigrid strategy with a generalized alternating direction method as a smoothing algorithm on each of the meshes. On each mesh, the flow field is alternately swept from the far field toward the airfoil surface and then sequentially along the upper and lower surfaces from leading to trailing edge. With the o-type meshes that we are using, the sweep directions follow the flow directions reasonably well in supersonic regions. Breakdown of the iteration scheme occurs only when the supersonic region extends all the way to the trailing edge. When this condition does not arise, the method works equally well with either difference scheme.

III. Results

All the flows that will be shown were computed on a 192 x 32 mesh, and a total of five mesh levels were employed in the multigrid sequence in each case. Each case was computed twice, once employing the flux biasing scheme and again using the density biasing scheme. The same set of ADI parameters was used for both calculations. In Fig. 1, the flow over the NACA0012 airfoil at a free stream Mach number of 0.720 and an angle of attack of 1° is depicted as computed by the two schemes. The shock on the upper surface is very weak in this case, as can be gathered from the very low drag values, and one can see how much better it is resolved by the flux biasing scheme. As we increase the Mach number and, thus, increase the strength of the shock, the shock capturing capability of the density biasing scheme as compared to the flux biasing scheme improves as we see from Fig. 2 and 3. With a still stronger shock at $M_\infty = 0.75$ and $\alpha = 2°$ (Fig. 4), we note that the differences between the two schemes become even smaller. In each of these cases the flux biasing scheme spreads out the jump from supersonic to subsonic conditions over three mesh intervals with most of the jump occurring in the middle one. The smearing with the density biasing scheme is more substantial with the weaker shocks but is drastically reduced as the shock strength increases. These observations are also borne out by comparisons of computations for the Korn airfoil at a Mach number of 0.70 for $\alpha = 1°$ and 2° (Fig. 5 and 6, respectively) and a Mach number of 0.75 for $\alpha = 0.2°$ and 0.7° (Fig. 7 and 8). Both schemes could be run throughout the range of applicability of the potential approximation. With only first order accuracy in the supersonic region ($v_2 \equiv 1$) both methods could be made to run until the shock reaches the trailing edge as seen in Fig. 9, which gives the Mach contours for the Korn airfoil at $M_\infty = 0.78$, $\alpha = 0.9°$. The pressures

3

computed by the two schemes are shown in Fig. 10. This case is included only for numerical interest since it is far beyond the physically acceptable limit of our assumptions. Overshoots develop ahead of the shock with both schemes.

	C_L	C_D	C_M
+ + + + FLUX BIASING	0.2038	0.0002	-0.0001
× × × × DENSITY BIASING	0.2038	0.0002	-0.0001

	C_L	C_D	C_M
+ + + + FLUX BIASING	0.2366	0.0026	-0.0007
× × × × DENSITY BIASING	0.2357	0.0023	-0.0005
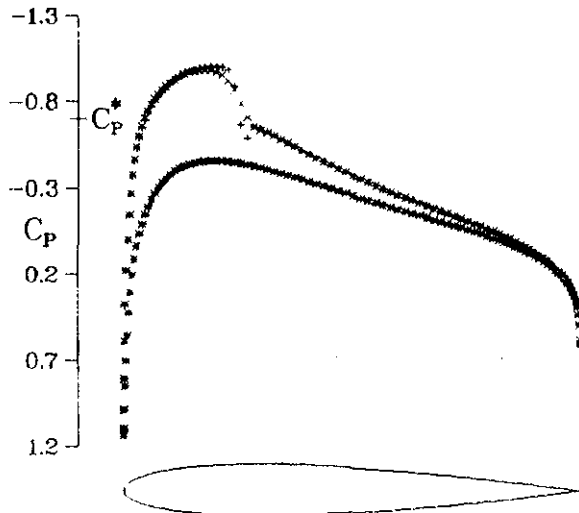
Fig. 1 Pressure distributions computed by flux biasing and density biasing schemes; NACA 0012 airfoil; $M_\infty = 0.720$, $\alpha = 1.0°$.
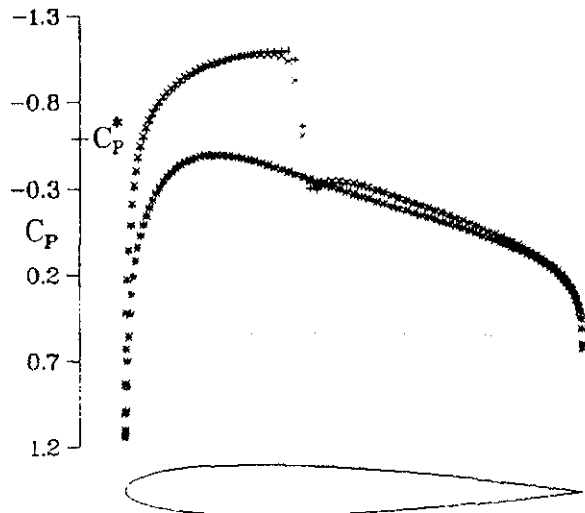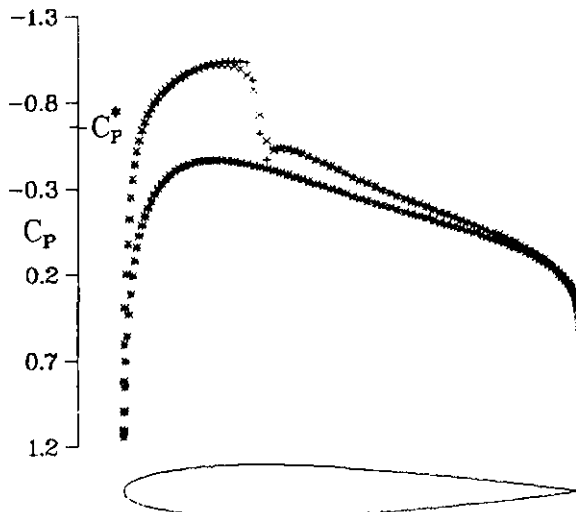

Fig. 3 Pressure distributions computed by flux biasing and density biasing schemes; NACA 0012 airfoil; $M_\infty = 0.750$, $\alpha = 1.0°$.
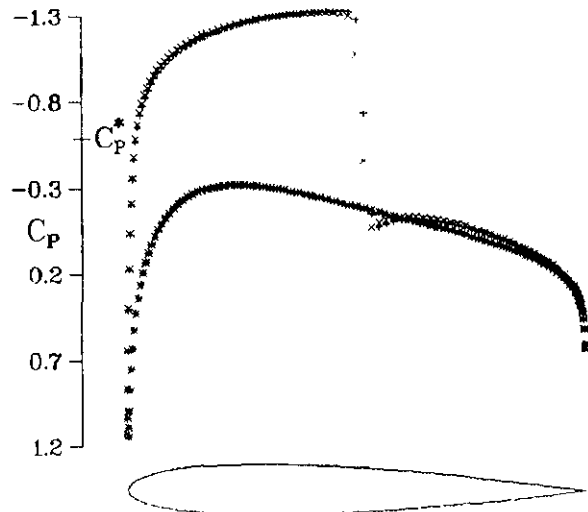
	C_L	C_D	C_M
+ + + + FLUX BIASING	0.2122	0.0006	0.0003
× × × × DENSITY BIASING	0.2120	0.0005	0.0003

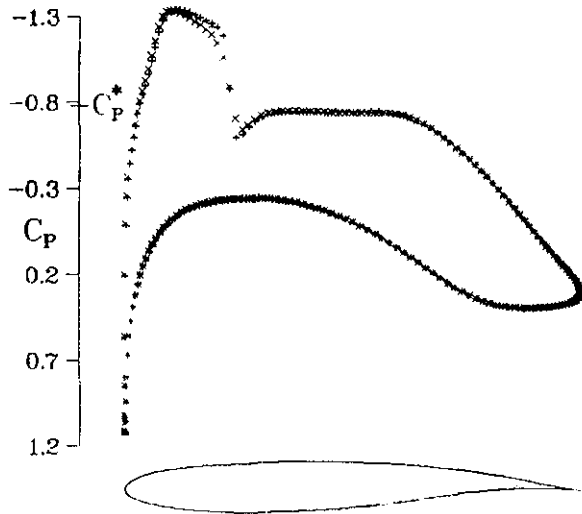|	C_L	C_D	C_M
+ + + + FLUX BIASING	0.5130	0.0158	-0.0166
× × × × DENSITY BIASING	0.5094	0.0147	-0.0148

Fig. 2 Pressure distributions computed by flux biasing and density biasing schemes; NACA 0012 airfoil; $M_\infty = 0.730$, $\alpha = 1.0°$.

Fig. 4 Pressure distributions computed by flux biasing and density biasing schemes; NACA 0012 airfoil; $M_\infty = 0.750$, $\alpha = 2.0°$.

4

	C_L	C_D	C_M
+ + + + FLUX BIASING	0.6986	0.0012	-0.1300
× × × × DENSITY BIASING	0.6980	0.0009	-0.1301

	C_L	C_D	C_M
+ + + + FLUX BIASING	0.6512	0.0003	-0.1474
× × × × DENSITY BIASING	0.6520	0.0006	-0.1493

Fig. 5 Pressure distributions computed by flux biasing and density biasing schemes; Korn airfoil; $M_\infty = 0.700, \alpha = 1.0°$.
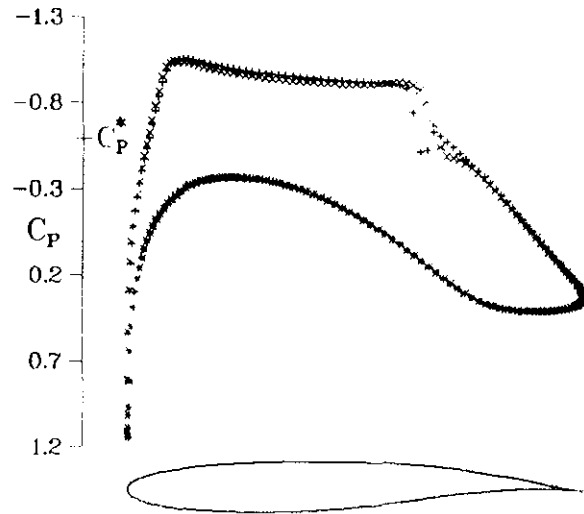
Fig. 7 Pressure distributions computed by flux biasing and density biasing schemes; Korn airfoil; $M_\infty = 0.750, \alpha = 0.2°$.

	C_L	C_D	C_M
+ + + + FLUX BIASING	0.9337	0.0062	-0.1292
× × × × DENSITY BIASING	0.9321	0.0054	-0.1285

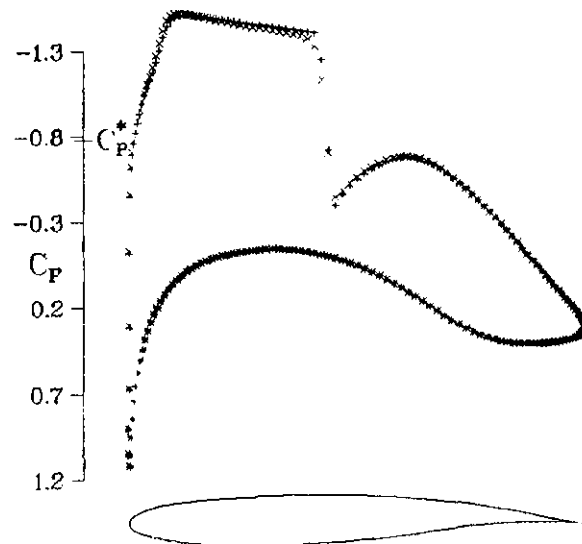|	C_L	C_D	C_M
+ + + + FLUX BIASING	0.8279	0.0072	-0.1712
× × × × DENSITY BIASING	0.8283	0.0068	-0.1711

Fig. 6 Pressure distributions computed by flux biasing and density biasing schemes; Korn airfoil; $M_\infty = 0.700, \alpha = 2.0°$.
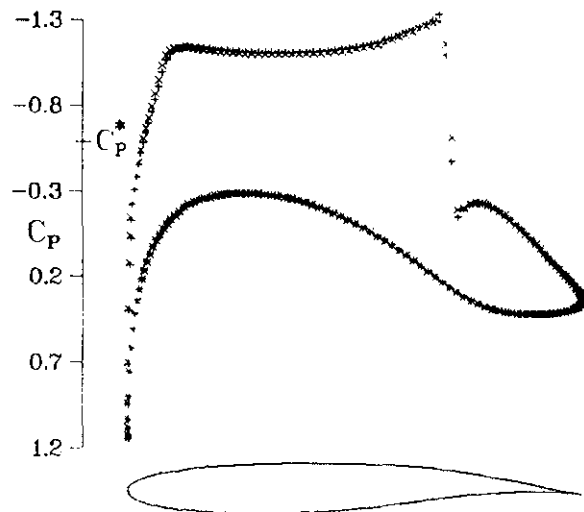
Fig. 8 Pressure distributions computed by flux biasing and density biasing schemes; Korn airfoil; $M_\infty = 0.750, \alpha = 0.7°$.

Fig. 9 Mach number contours computed by flux biasing scheme; Korn airfoil; $M_\infty = 0.780$, $\alpha = 0.9°$.

	C_L	C_D	C_M
+ + + + FLUX BIASING	1.3084	0.0941	-0.4388
× × × × DENSITY BIASING	1.3192	0.0939	-0.4416

Fig. 10 Pressure distributions computed by flux biasing and density biasing schemes; Korn airfoil; $M_\infty = 0.780$, $\alpha = 0.9°$.
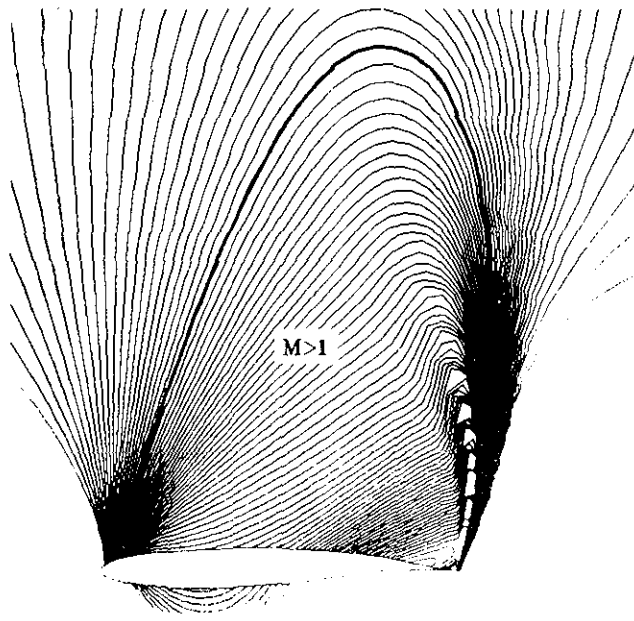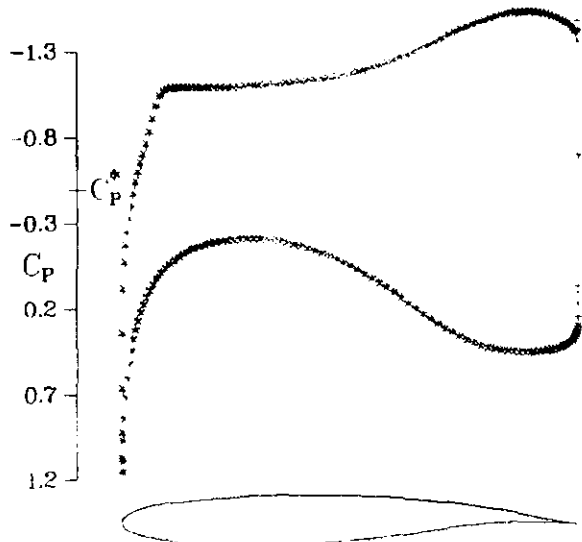
Table 1 gives the number of cycles needed to obtain convergence, defined as attainment of a specified value in the maximum residual. In most cases, the density biasing scheme is marginally faster. The flux biasing scheme shows a substantial advantage only in the last example. As mentioned above, runs were made with the same set of ADI parameters for both dissipation schemes. It is possible that convergence might be speeded up for either scheme with different parameters.

Table 1 Cycles required for convergence

Airfoil	M_∞	α	Flux Biasing	Density Biasing
NACA 0012	0.720	1.0°	19	13
NACA 0012	0.730	1.0°	17	15
NACA 0012	0.750	1.0°	19	24
NACA 0012	0.750	2.0°	59	55
Korn Airfoil	0.700	1.0°	25	18
Korn Airfoil	0.700	2.0°	43	43
Korn Airfoil	0.750	0.2°	39	41
Korn Airfoil	0.750	0.7°	108	95
Korn Airfoil	0.780	0.9°	138	260

IV. Concluding Remarks

Two second order accurate forms of artificial dissipation based on density biasing and flux biasing have been introduced in an otherwise identical numerical method for computing the steady transonic flow over an airfoil. The numerical experiments have shown that the two schemes are equally robust and have similar convergence qualities. For weak shock waves, the flux biasing scheme gives a sharper definition of the shock than the density biasing scheme. In all cases, the former scheme captures most of the jump in one mesh interval and all of it within three intervals. The density biasing scheme shock-capturing ability improves with increasing shock strength and equals that of the other scheme for strong shock waves. This smearing is apparently due to the need to switch on the dissipation at a Mach number lower than one in the density biasing method to enhance stability. The attractive feature of the flux biasing method is the fact that the dissipation is needed only at supersonic points.

References

1. Jameson, A., "Acceleration of Transonic Potential Flow Calculations on Arbitrary Meshes by the Multiple Grid Method," AIAA Paper 79-1458, 1979.

2. Holst, T., "Implicit Algorithm for the Conservative Transonic Full Potential Equation Using an Arbitrary Mesh," AIAA J., Vol. 17, No. 10, pp. 1038-1045, 1979.

3. Melnik, R. E., and Brook, J. W., "The Computation of Viscid/Inviscid Interaction on Airfoils with Separated Flow," presented at Third Symposium on Numerical and Physical Aspects of Aerodynamic Flows held at California State Univ., Jan. 1985.

4. Hafez, M. M., Murman, E. M., and South, J. E., "Artificial Compressibility Methods for Numerical Solution of Transonic Full Potential Equation," AIAA Paper 78-1148, 1978.

5. Boerstoel, J. W., "A Multigrid Algorithm for Steady Transonic Potential Flows around Airfoils Using Newton's Iteration," J. Comp. Phys., Vol. 48, pp. 313-343, 1982.

6. Hafez, M. M., Osher, S., and Whitlow, W., "Improved Finite Difference Schemes for Transonic Potential Calculations," AIAA Paper 84-0092, 1984.

7. Engquist, B., and Osher, S., "Stable and Entropy Satisfying Approximations for Transonic Flow Calculations," Math. Comp., Vol. 34, No. 149, pp. 45-75, 1980.

8. Osher, S., Hafez, M., and Whitlow, W., "Entropy Satisfying Approximations for the Full Potential Equation of Transonic Flow," Math. Comp., Vol. 44, No. 169, pp. 1-29, 1985.

9. Hafez, M., and Lovell, D., "Entropy and Vorticity Corrections for Transonic Flows," AIAA Paper 83-1926, 1983.